Journal Pre-proofs

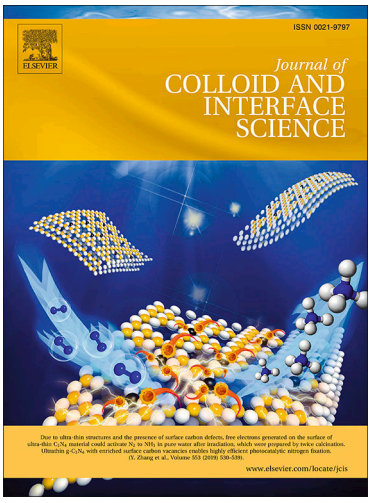

Regular Article

Polylysine-modified MXene nanosheets with highly loaded glucose oxidase as cascade nanoreactor for glucose decomposition and electrochemical sensing

Minying Wu, Qian Zhang, Yuanyuan Fang, Chao Deng, Fangzhou Zhou, Yi Zhang, Xingdong Wang, Yi Tang, Yajun Wang

PII: S0021-9797(20)31405-3
DOI: https://doi.org/10.1016/j.jcis.2020.10.065
Reference: YJCIS 27096

To appear in: *Journal of Colloid and Interface Science*

Received Date: 5 August 2020
Revised Date: 17 October 2020
Accepted Date: 19 October 2020

Please cite this article as: M. Wu, Q. Zhang, Y. Fang, C. Deng, F. Zhou, Y. Zhang, X. Wang, Y. Tang, Y. Wang, Polylysine-modified MXene nanosheets with highly loaded glucose oxidase as cascade nanoreactor for glucose decomposition and electrochemical sensing, *Journal of Colloid and Interface Science* (2020), doi: https://doi.org/10.1016/j.jcis.2020.10.065

This is a PDF file of an article that has undergone enhancements after acceptance, such as the addition of a cover page and metadata, and formatting for readability, but it is not yet the definitive version of record. This version will undergo additional copyediting, typesetting and review before it is published in its final form, but we are providing this version to give early visibility of the article. Please note that, during the production process, errors may be discovered which could affect the content, and all legal disclaimers that apply to the journal pertain.

© 2020 Elsevier Inc. All rights reserved.

Polylysine-modified MXene nanosheets with highly loaded glucose oxidase as cascade nanoreactor for glucose decomposition and electrochemical sensing

Minying Wu,[a] Qian Zhang,[a] Yuanyuan Fang,[a] Chao Deng,*[b] Fangzhou Zhou,[a] Yi Zhang,*[c] Xingdong Wang,[d] Yi Tang,[a] and Yajun Wang*[a,b]

[a.]Department of Chemistry, Fudan University, Shanghai, 200433, P. R. China. E-mail: yajunwang@fudan.edu.cn

[b.]College of Chemistry & Materials Engineering, Wenzhou University, Wenzhou 325027, Zhejiang, P. R. China. E-mail: dengchao@wzu.edu.cn

[c.]School of Materials Science and Energy Engineering, Foshan University, Foshan 528000, Guangdong, P. R. China. E-mail: imzhy@fosu.edu.cn

[d.]CSIRO Manufacturing, Private Bag 10, Clayton South, Victoria 3169, Australia.

Abstract

Two-dimensional (2D) nanoreactors with cascade catalytic activity for glucose oxidation and hydrogen peroxide decomposition are prepared via immobilizing glucose oxidase (GOx) on Ti_3C_2 MXene nanosheets. Amino-rich polypeptide, poly-L-lysine (PLL), is applied to modify the ultra-thin Ti_3C_2 MXene nanosheets with a compatible surface for GOx immobilization. The PLL-modified Ti_3C_2 nanosheets possess a positively charged surface and show show an excellent GOx loading capacity as high as 50 wt.% of the Ti_3C_2 nanosheets. The physically adsorbed enzymes are then cross-linked with the amine groups in the PLL chains to form a robust GOx-PLL network covered on the MXene nanosheets. The GOx-conjugated Ti_3C_2-PLL (Ti_3C_2-PLL-GOx) nanosheets showed superior enzymatic activities than the activities of GOx

immobilized on an inert porous silica substrate, largely because that the Ti_3C_2 nanosheets can catalyze the decomposition of the toxic intermediate H_2O_2 generated from the glucose oxidation. Given the excellent electrical conductivity of Ti_3C_2 MXene, the Ti_3C_2-PLL-GOx nanosheets are further deposited on glassy carbon electrode to construct a high-performance biosensor with a glucose detection limit 2.6 μM.

Introduction

Glucose oxidase (GOx) is a flavoenzyme, which utilizes molecular oxygen as the main electron acceptor to catalyze the oxidation of β-D-glucose to D-glucono-δ-lactone and to generate hydrogen peroxide (H_2O_2).[1-3] GOx has been used in various applications, ranging from biosensing,[4-8] to diabetes detection,[9, 10] anticancer therapy[11-13] and glucose fuel cell.[14, 15] However, the toxic intermediate product (H_2O_2) generated during the enzymatic glucose oxidation often inhibits the activity of GOx in practical applications.[16] To tackle this issue, a strategy of constructing a cascade reaction system that induces the decomposition of the intermediate by-product H_2O_2 has been proposed.[11] The enzymatic cascade reaction typically involves two different types of enzyme,[17, 18] the first enzyme is used to catalyze the main reaction while the second enzyme is applied to break down the intermediate products. However, the use of multiple enzymes in the system will bring complicated issues and is not cost-effective.[19] It would be interesting if the substrate used for GOx immobilization could simultaneously have the properties for H_2O_2 decomposition.

MXenes, a new family of two-dimensional (2D) transition metal carbides, nitrides,

or carbonitrides,[20, 21] have recently gained tremendous attention, because of their extraordinary physical and chemical properties (e.g., excellent electrical conductivity, high aspect ratio, large surface area, and hydrophilicity).[22-24] The MXene nanosheets are prepared by selective etching of the A element layers from the MAX phases, that is, $M_{n+1}AX_n$, where M is an early transition metal (e.g., Ti, Zr, V, Ta, Nb, Mo, etc.), A belongs mainly to a group IIIA or IVA element, and X corresponds to carbon and/or nitrogen. The etching off of A layer by F-containing etchants results in the replacement of A element with other surface termination groups (e.g., OH, F, and/or O). Thereafter, MXenes with typical formula of $M_{n+1}X_nT_x$ will be obtained, where T_x corresponds to the terminated groups. As a result, diverse MXenes with different properties can be synthesized by rational combination of M and X atoms, and the surface-terminated T_x groups. Owing to their unique structural, physicochemical, and compositional features,[22-24] MXenes have been widely studied in a range of applications such as catalysis,[25, 26] energy storage,[27] nanomedicine,[28] electromagnetic shielding,[29] sensing[30, 31] and water treatment.[32] Ti_3C_2 MXene, the first and most widely studied in the MXene family, has been prepared through selective etching of Al from the Ti_3AlC_2 MAX parent phase.[33-35] By using its excellent electrical conductivity properties, Ti_3C_2 MXene has been used to support metal nanoparticles[36] or hemoglobin (Hb)[37] for electrochemical sensing of H_2O_2. Recently, Lorencova et al. reported that the Ti_3C_2 MXene was also able to catalyze the decomposition reaction of H_2O_2.[24]

Taking advantages of the H_2O_2 catalytic decomposition properties and high specific surface area of Ti_3C_2 MXene, here, we propose a novel 2D cascade nanoreactor through immobilizing GOx on poly-L-lysine (PLL)-modified Ti_3C_2 MXene (denoted as Ti_3C_2-PLL-GOx) (**Scheme 1**). The amino-rich PLL is used to modify the Ti_3C_2 nanosheets with a layer of positively-charged polypeptide, which can be used to electrostatically adsorb the negatively charged GOx.[38] The physically adsorbed enzymes are then cross-linked with the amine groups in PLL chains to form a robust GOx-PLL network covered on the Ti_3C_2 MXene nanosheets. Superior catalytic performance of GOx is obtained on the Ti_3C_2-PLL-GOx nanoreactors due to the GOx and the Ti_3C_2 nanosheets can form a cascade reaction in glucose decomposition. The oxygen produced from H_2O_2 decomposition under the catalysis of Ti_3C_2 nanosheets can be re-used in the glucose oxidation reaction, which in turn increased the reaction rates of the glucose oxidation. Taking advantage of the excellent electrical conductivity of Ti_3C_2, the Ti_3C_2-PLL-GOx nanosheets are further deposited on glassy carbon electrodes to construct high-performance electrodes for glucose sensing with a detection limit of 2.6 μM.

Experimental Section

Chemicals:

Poly-L-lysine hydrobromide (M*w* 30-70 kDa), GOx (from *Aspergillus niger*, 127 U mg^{-1}), horseradish peroxidase (HRP, >200 U mg^{-1}), 3, 3’ ,5, 5’-tetramethylbenzidine (TMB), N-(3-dimethylaminopropyl)-N’-ethylcarbodiimide hydrochloride (EDC), 2-morpholinoethanesulfonic acid monohydrate (MES) and H_2O_2 were purchased from

Sigma-Aldrich Inc. Ti_3AlC_2 was purchased from Forsman Technology (Beijing) Co., Ltd.. Lithium fluoride (LiF), acetic acid (HAc), sodium acetate (NaAC) and hydrochloric acid (HCl) (36.0-38.0%) were purchased from Sinopharm Chemical Reagent Co. Ltd. D-(+)-Glucose was obtained from Aladdin (China). N-methylpyrrolidone (NMP) was obtained from General-Reagent Inc (China). All reagents used were analytical grade without further purification.

Synthesis of Ti_3C_2 Nanosheets:

The Ti_3C_2 nanosheets were prepared by a method adapted from literature.[39, 40] In brief, 2.0 g of Ti_3AlC_2 powder was slowly added to a mixed solution of 2.0 g of LiF and 20 ml of HCl. The reaction was maintained at 50 °C for 48 h in an oil bath under magnetic stirring. Then, the suspension was centrifuged (2600 *g*, 5 min) and washed several times with deionized water until pH of the supernatant was around 6. After that, the precipitate was redispersed in 40 mL of NMP and sonicated for 8 h with a probe sonication. The power of the sonication was 260 W, while the working time and interval time of the probe was set as 4 s and 2 s, respectively. During the sonication process, temperature of the solution was maintained below 277 K by using an ice bath. Finally, the Ti_3C_2 nanosheets were freeze-dried after centrifuging and removal of the supernatant.

Assembly of Hybrid Ti_3C_2-PLL-GOx Nanosheets:

Typically, 0.5 mL of 1.0 mg mL^{-1} PLL stock solution (pH 5.5, 50 mM MES) was added to 0.5 mL of 1.0 mg mL^{-1} Ti_3C_2 suspension. The mixture was shaken at room

temperature for 1 h. The PLL-modified Ti_3C_2 (denoted as Ti_3C_2-PLL) was collected by centrifugation (16000 *g*, 5 min), and washed with MES buffer (50 mM, pH 5.5) twice, following by redispersion in 0.5 mL of MES buffer. Then, 0.5 mL of GOx stock solution (pH 5.5, 50 mM MES) with enzyme concentration of 1.0 mg mL^{-1} was added to above Ti_3C_2-PLL suspension and shaken at room temperature for 1 h. After removal of the excess GOx via centrifugal separation, 0.5 mg of EDC (10 mg mL^{-1} in 50 mM MES, pH 5.5) was added and incubated at room temperature for 1 h to conjugate the residual carboxyl groups in GOx with the amino groups in PLL chains. The obtained materials were washed with MES buffer twice and finally distributed in 0.5 mL of HAc-NaAc buffer (50 mM, pH 5).

Enzymatic Activity Assay:

Free or immobilized GOx with a GOx content of 5.0 μg was added to 2.0 mL of 11.5 mM glucose solution (pH 5, 50 mM HAc-NaAc buffer). The reaction was maintained at 40 °C and stopped after 0.5 h by adding 50 μL of 2.0 M H_2SO_4 solution. With reference to the standard curves of glucose (Figure S1) and H_2O_2 (Figure S2), A colorimetric method adopting a combination of HRP and TMB was used to determine the glucose concentration and H_2O_2 concentration in the reaction solution.[41, 42] Detailed procedures for these measurements were summarized in the supporting information.

Preparation of Ti_3C_2-PLL-GOx/GCE Electrode:

The bare glassy carbon electrode (GCE) was cleaned with a mixed solution of water

and ethanol (1:1 v/v), and then sequentially polished with 1.0 μm, 0.3 μm, and 0.05 μm alumina powder on microcloth pads. The polished GCE was ultrasonically cleaned three times (2 min each time) with a mixed water-alcohol solution. 5.0 μl of the Ti_3C_2-PLL-GOx suspension (1.0 mg mL^{-1}) was deposited on the GCE surface and dried naturally at room temperature to obtain the Ti_3C_2-PLL-GOx/GCE electrode.

Characterization:

Transmission electron microscope (TEM) images were obtained on a Hitachi H-600 TEM operating at 200 kV. Scanning electron microscope (SEM) measurements were conducted on an Ultra 55 field emission microscope (SEM, Zeiss, Germany) operating at 5 kV. Energy dispersive X-ray (EDX) spectroscopy element mapping was carried out on a Tecnai G2 F20 S-Twin STEM instrument (FEI, Hillsboro, OR). Zeta potential was measured by Zetasizer Nano-ZS (Malvern). Fourier transform infrared (FTIR) spectra were collected on Spectrum Two FT-IR spectrometer (PerkinEImer). Raman spectra were measured using a Super LabRam Raman spectrometer (50% laser power, acq. time: 10 s, accumulation: 3). He-Ne laser with an excitation wavelength of 514 nm was used. A 50× long distance objective lens was used for the Raman measurements. X-ray diffraction (XRD) patterns were measured on a Bruker AXS D2 PHASER diffractometer using Cu K_α radiation (λ = 1.54056 Å, 40 kV, 40 mA). The scanning range is from 5° to 90° (time: 1 s, increment: 0.004, scan mode: continuous PSD fast). UV-vis spectra were collected on a Shimadzu UV-2600 spectrophotometer to monitor the enzyme loading and assay the enzyme activity. A Bruker Dimension Fast Scan

Atomic Microscope was used to measure the AFM images in tapping mode. The sample was dispersed in H_2O solution and deposited on silicon wafer for testing. Electrochemical related tests were performed with a CHI 660D electrochemical analyzer (Chenhua, China). A conventional three-electrode system was used for electrochemical experiments, which consisted of a platinum wire as auxiliary electrode, an Ag/AgCl/saturated KCl as reference electrode, and the self-prepared Ti_3C_2-PLL-GOx/GCE as working electrode. The cyclic voltammogram (CV) measurement employed a scan rate of 100 mV s^{-1}.

Results and Discussion

The procedure used for the Ti_3C_2-PLL-GOx nanoreactor preparation was illustrated in **Scheme 1**. The Ti_3C_2 MXene was obtained through etching out the Al from Ti_3AlC_2 and then separating the obtained multi-layered Ti_3C_2 to ultrathin nanosheets by a probe sonication (Scheme 1a). PLL, a polypeptide with abundant amino groups in the chain, was used to modify the Ti_3C_2 nanosheets with a positively charged surface (Scheme 1b). Lysine is an essential amino acid with two amino groups, α and ε, which have pK values of 8.95 and 10.53, respectively. PLL, formed by the polymerization of lysine, has advantages of abundant amino groups, good biocompatibility, flexible molecular framework and relatively good solubility in water,[43] for electrode modification to develop electrochemical biosensors.[44-46] The GOx molecules were electrostatically adsorbed on the PLL-modified Ti_3C_2 nanosheets and cross-linked together with the PLL chains to form a GOx-PLL network on the MXene surface.

The original Ti_3AlC_2 powder possessed a compact layered structure (**Figure 1a**). Multi-layered Ti_3C_2 flakes were produced after etching the Al layers from Ti_3AlC_2 with LiF/HCl (Figure 1b). After sonication of the multi-layered Ti_3C_2 suspension in N-methyl pyrrolidone, ultra-thin Ti_3C_2 nanosheets with a dimension of *ca.* 200 nm were obtained (Figure 1c).[39] The Ti_3C_2 nanosheets could be well dispersed in aqueous solution, and showed clear Tyndall effect as displayed in the digital photo inserted in Figure1c. High resolution TEM (HRTEM) image revealed that the spacing between two adjacent lattice fringes was 0.265 nm (Figure 1d), corresponding to the $(01\bar{1}0)$ plane of the Ti_3C_2 crystal.[47-49] The precursor Ti_3AlC_2 is a hexagonal crystal system and the space group is $P6_3/mmc$. Its structure can be seen as a symbiotic structure composed of hexagonal Ti_3C_2 layers and plane Al atomic sheets alternately stacking along the c axis.[23] The inset in Figure 1d was the selected area electron diffraction (SAED) pattern of Ti_3C_2, which further demonstrated that the lattice plane is hexagonal symmetric.[50] Thickness of the Ti_3C_2 nanosheets was estimated to be approximately 1.2-2.5 nm as measured from the AFM diagram (Figure 1e, f), suggesting the Ti_3C_2 nanosheets had a single- or few-layered structure.[51] The theoretical thickness of a single-layer Ti_3C_2 flake is 0.98 nm.[52] The higher thickness determined from AFM might be due to the H_2O molecules being trapped between the Ti_3C_2 nanosheet and the substrate.[21, 53]

XRD characterization was used to monitor the phase changes of the materials. The Ti_3AlC_2 powder had a strong diffraction peak at 39.0° (Figure 1g), which could be

corresponded to the (104) diffraction peak of Ti_3AlC_2 (jade card # 52-0875). The weak diffraction peaks (* marked) at 13.0° and 35.9° could be attributed to small amount of Ti_2AlC (jade card # 29-0095) and TiC (jade card # 32-1383) phases co-existed in the commercial Ti_3AlC_2 powder (Figure S3). The Ti_3AlC_2 MAX phase was estimated to be 95.03 wt.% by Rietveld refinement method. The strong diffraction peak at 39.0° totally disappeared in the Ti_3C_2 nanosheets, suggesting that the Al layer in the MAX phase was efficiently etched. In addition, the (002) diffraction peak was broadened and shifted from 9.6° to 6.6°, indicating an increase of the c-lattice parameter from 1.8 nm to 2.7 nm. This is consistent with the c-lattice parameter (2.7-2.8 nm) of Ti_3C_2 MXene prepared at similar etching conditions (LiF/ HCl, 40 ℃, 45 h).[40] Raman spectra of the Ti_3C_2 nanosheets were shown in Figure 1h. The A_{1g} symmetry vibrations of Ti and C atoms occurred at 209 cm^{-1} (ω2) and 728 cm^{-1} (ω3). The in-plane (shear) modes (Eg groups) of Ti, C and surface functional group atoms were at 288 (ω5), 388 (ω5) and 622 cm^{-1} (ω4), respectively.[54, 55] A broad near-infrared (NIR) light absorption peak at 808 nm occurred in the Ti_3C_2 MXene (Figure 1i), coincided with the results reported previously.[56]

The enzyme loading was performed by incubating GOx with the nanosheets at a mass ratio of 1:1. The enzyme loaded was determined by monitoring the GOx concentration in the supernatant via UV-vis spectrophotometry. Influence of the PLL-modification and solution pH on GOx loading was also investigated. As shown in Figure 2a, GOx had a saturated loading of *ca.* 3.2% and 18.7% on the as-prepared Ti_3C_2 nanosheets in

H_2O solution (pH 6.7) and pH 5.5 MES buffer, respectively. After PLL modification, loading capacity of the MXene nanosheets to GOx was significantly improved, with a saturated loading of *ca.* 42.7 wt.% and 50.4 wt.% in H_2O solution and MES buffer, respectively. These data demonstrated that the PLL modification played important roles in improving the GOx loading on MXenes. PLL is positively charged and the charge density of the polymer is increased with the solution pH decreases, which provides stronger electrostatic attraction between the PLL molecules and the negatively charged Ti_3C_2 MXene or GOx molecules. Also, having an isoelectric point (IEP) of 4.2,[57] GOx is negatively charged in the loading conditions and the surface electronegativity of GOx will be decreased with the solution pH close to its IEP, which reduces the electrostatic repulsion among the GOx molecules. Thereafter, the GOx molecules could be adsorbed more compactly on the substrates when the loading experiments were carried out in pH 5.5 MES buffer.

Geometrical impacts of the substrate on enzyme loading was also investigated through comparing the GOx loading on 2D nanosheets and 3D porous particles. The bimodal mesoporous silica (BMS) spheres with highly porous structures for enzyme loading,[58, 59] were used as a model porous particle. As shown in Figure 2b, loading of GOx on the Ti_3C_2 nanosheets was very fast and saturated in a few minutes. In addition, the enzyme loading on the Ti_3C_2 nanosheets is also much higher (~five times) than that obtained in the porous particles (Figure 2b, insert). The quicker and higher enzyme loading on the 2D nanosheets could be mainly attributed to the larger and easily

accessible external surface of the Ti_3C_2 nanosheets.

The loading of GOx on Ti_3C_2-PLL nanosheets could also be indicated from the alternatively positive and negative variations of the surface charge. Zeta potential measurements were performed to monitor the surface charge variations of the nanosheets after each step of process. The pristine Ti_3C_2 nanosheets were negatively charged, with a zeta potential of -26.2 mV (**Figure 3a**). After PLL modification, zeta potential of the nanosheets changed to +28.7 mV, indicating successful modification of the polycationic PLL on the Ti_3C_2 nanosheets. After loading of the negatively charged GOx, zeta potential of the Ti_3C_2-PLL nanosheets shifted to -20.3 mV.

FTIR spectra of the Ti_3C_2, Ti_3C_2-PLL, and Ti_3C_2-PLL-GOx were shown in figure 3b. The peak with a wavenumber of 1685 cm^{-1}, attributed to the amide I bond (1700-1600 cm^{-1}), was caused by the stretching vibration of C=O at the junction of the peptide in the backbone of the GOx peptide and PLL chains. The amide II bond with a wavenumber of 1566 cm^{-1} in the FTIR spectra was originated from the bending of N-H and the stretching vibration of C-N.[60]

The Ti_3C_2-PLL and Ti_3C_2-PLL-GOx nanosheets maintained similar morphology and dispersibility as the original Ti_3C_2 nanosheets (**Figure 4a-c**). Elemental mapping profiles were further used to monitor the distribution of PLL and GOx on the nanosheets. The PLL-modified Ti_3C_2 nanosheets showed uniform N element distribution (Figure S4), demonstrating that PLL was homogeneously adsorbed on the Ti_3C_2 nanosheets. Homogeneous distribution of GOx on the nanosheets was demonstrated from the P

elemental mapping profiles of the Ti_3C_2-PLL-GOx nanosheets (Figure 4d). As determined from the EDX patterns of the samples (Figure S5), contents of the N and P element in the nanosheets was also obtained in Table S1.

Bioactivity of the immobilized GOx was investigated through the enzymatic oxidation of glucose. The influence of enzyme loading on their bioactivity was studied by using Ti_3C_2-PLL-GOx nanosheets with different GOx loading (5, 10, 30, and 50 wt.%), which were prepared through mixing the Ti_3C_2-PLL nanosheets with different amount of GOx in the incubation solution during the enzyme loading process. Equivalent amount of GOx (5.0 μg) was used in the enzymatic activity study and activity of the free GOx was nominalized as 100%. The results showed that the enzyme activity gradually decreased with the increasement of GOx loading (**Figure 5a**). The Ti_3C_2-PLL-GOx nanosheets with the highest GOx loading (50 wt.%) had the lowest relative activity (77.8%), likely because that some active sites of GOx might be blocked in the compactly immobilized enzyme molecules. Further decrease of the GOx loading below 10 wt% would not improve the enzymatic activity much. Ti_3C_2-PLL-GOx nanosheets with 5 and 10 wt.% of GOx loading had a similar relative activity of 85.1% and 84.5%. Thereafter, Ti_3C_2-PLL-GOx nanosheets with a 10 wt.% of GOx loading would be used in following experiments.

The catalyzed H_2O_2 decomposition capacity of Ti_3C_2 nanosheets was demonstrated from the continuous decrease of the H_2O_2 concentration when the Ti_3C_2 nanosheets were added into the H_2O_2 solution (Figure 5b). The amount of H_2O_2 decomposed in the

system was evaluated to be approximately 0.79 mM in 4 h. Therefore, in addition to acting as a substrate for GOx immobilization, the H_2O_2 decomposition properties of Ti_3C_2 nanosheets could be simultaneously applied in the GOx involved cascade reaction for glucose oxidation.

As shown in Formula 1, under the catalysis of GOx, one molecule of glucose reacted with one molecule of oxygen to produce one molecule of gluconolactone and H_2O_2. The generated H_2O_2 could be degraded into H_2O and O_2 by Ti_3C_2 nanosheets (Formula 2). Thereafter, the oxidation of glucose by Ti_3C_2-PLL-GOx formed a cascade reaction. The generated oxygen was recyclable in the glucose oxidation reaction, showing interesting synergies.

$$\text{glucose} + O_2 \xrightarrow{\text{GOx}} \text{gluconolactone} + H_2O_2 \quad (1)$$

$$H_2O_2 \xrightarrow{Ti_3C_2} H_2O + \frac{1}{2}O_2 \quad (2)$$

To evaluate the synergetic effects of the Ti_3C_2 nanosheets on GOx catalyzed glucose oxidation, GOx immobilized on an inert mesoporous silica substrate (denoted as BMS-PLL-GOx) was also compared. The BMS-PLL-GOx particles were prepared via the same procedure used for Ti_3C_2-PLL-GOx preparation with the details summarized in the supporting information. Influence of the cascade produced O_2 on the catalytic activity of GOx was investigated in a closed environment, in which the reaction was isolated from the atmosphere by adding a layer of n-hexane on top of the nitrogen-saturated solution to avoid the influence of atmosphere O_2 in the reaction. During the first hour of reaction, the Ti_3C_2-PLL-GOx degraded 2.09 mM of glucose (Figure 5c),

corresponding to an enzymatic activity of 3.47 U. In comparison, BMS-PLL-GOx degraded much less glucose (1.48 mM) with a calculated enzymatic activity of 2.46 U. In a total reaction time of 4 h, Ti_3C_2-PLL-GOx and BMS-PLL-GOx had decomposed 3.48 mM and 2.86 mM of glucose, respectively.

In the GOx catalyzed glucose oxidation reaction, more H_2O_2 would be generated when more glucose molecules were reacted. As we mentioned above, the catalyst of Ti_3C_2-PLL-GOx degraded 0.61 mM more glucose than the BMS-PLL-GOx system in the first hour of reaction (Figure 5c), thereafter, 0.61 mM more H_2O_2 should be detected in the former system. However, amount of H_2O_2 detected in the Ti_3C_2-PLL-GOx nanoreactors was significantly less. Also, the differences of H_2O_2 concentrations gradually increased with the reaction went on (Figure 5d). These results demonstrated that the Ti_3C_2 nanosheets could form a cascade reaction to degrade the H_2O_2 generated in glucose oxidation. The oxygen produced from H_2O_2 decomposition was able to be re-used in the glucose oxidation reaction, thereafter, promote the GOx catalyzed glucose oxidation reaction.

The reusability of the Ti_3C_2-PLL-GOx nanoreactor was also studied. After six successive batch reactions, GOx immobilized on the Ti_3C_2-PLL nanosheets retained 81% of its initial enzymatic activity (**Figure 6**). On contrary, GOx adsorbed on the Ti_3C_2 nanosheets only had 47% activity left. These data demonstrated that the PLL modification can not only significantly enhance the loading capacity of GOx on Ti_3C_2 nanosheets, but also suppress the activity loss of the enzyme during the cyclic using.

In fabrication of electrochemical biosensors, the realization of direct electron transfer (DET) between enzymes and electrodes is of great significance.[61] However, it is very challenging to achieve the DET between the protein and the electrode surface because the redox active center of the protein is embedded in the protein's shell.[62] Therefore, using conductive nanomaterials to promote DET of immobilized enzymes had been proposed in designing of electrochemical biosensors.[63] Owing to the excellent electrical conductivity, Ti_3C_2 MXene had been investigated in the preparation of electrode materials.[64] Hence, application of the Ti_3C_2-PLL-GOx nanosheets in electrochemical sensing was further investigated.

To evaluate the performance of Ti_3C_2-PLL-GOx nanosheets for glucose sensing, the Ti_3C_2-PLL-GOx nanosheets were drip-coated on a GCE to obtain an electrochemical biosensor. In principle, the electron transfer behavior could be deduced from a typical Nyquist spectrum. The charge transfer resistance (R_{ct}) of the sensing material could be measured from the diameter of the semicircular part in the electrochemical impedance spectroscopy (EIS) diagram. Therefore, the electron transfer process at the electrode interface could be detected through the reversible redox reaction in $K_3[Fe(CN)_6]/K_4[Fe(CN)_6]$ solution. Here, four electrodes of bare GCE, Ti_3C_2/GCE, Ti_3C_2-PLL/GCE, and Ti_3C_2-PLL-GOx/GCE were tested for impedance (**Figure 7**a). The specific R_{ct} value was obtained by simulation according to the equivalent circuit inserted. The resistance of the bare GCE was about 70.82 Ω. The Ti_3C_2/GCE electrode had a resistance of only 2.26 Ω, reflecting the excellent electrical conductivity of the Ti_3C_2 nanosheets. Using

the highly electrically conductive Ti_3C_2 substrate for enzyme immobilization was of benefit to accelerating the electron transport speed in the glucose biosensor, thereby improving the detection sensitivity. After sequential loading of the non-conductive PLL and enzyme, resistance of the Ti_3C_2-PLL/GCE, and Ti_3C_2-PLL-GOx/GCE was determined to be 37.81 Ω and 137.81 Ω, respectively.

The Ti_3C_2-PLL-GOx electrodes were tested in phosphate buffer saline (PBS) solution (0.1 M, pH 7.4) at different scan rates with cyclic voltammetry (CV) method. The reduction peak current increased as the scan rate increased (Figure 7b, inset). The peak current was proportional to the half power of the scanning speed with a linear regression equation: $I\ (\mu A) = -1.0246V^{1/2}((mV/s)^{1/2}) + 0.2055$ ($R^2 = 0.99995$), reflecting a diffusion control process.

Performance of the Ti_3C_2-PLL-GOx/GCE as working electrode toward glucose sensing was evaluated in a three-electrode system. With the continuous addition of glucose into the test solution, the test was performed using CV measurement. The magnitude of the current at the reduction peak decreased with glucose concentration increasing (Figure 8a, b, inset). This could be attributed to that the enzymatic decomposition of glucose would consume O_2 in the biosensor system, resulting in the decline of O_2 reduction current. The linear range for glucose detection consisted two segments. The first linear range is for glucose with a concentration range of 4.0-20 μM, the linear curve is $I\ (\mu A) = 5.0481C\ (mM) - 12.640$ (R^2=0.9999) (**Figure 8a**). The second range for glucose detection was 0.02-1.1 mM, with the linear curve to be I (μA)

= 2.6988C (mM) -12.539 (R^2=0.9981) (Figure 8b). The detection limit of the Ti_3C_2-PLL-GOx/GCE electrode for glucose determination was 2.6 μM. Given a diameter of 3 mm for the GCE electrode, the detection sensitivities of the two linear ranges were calculated to be 71.42 μA mM^{-1} cm^{-2} and 38.18 μA mM^{-1} cm^{-2}, respectively, significantly higher than the detection sensitivity of 4.2 μA mM^{-1} cm^{-2} reported on the GOx/Au/MXene/Nafion/GCE electrode.[65] Meanwhile, higher accuracy was also achieved from the Ti_3C_2-PLL-GOx/GCE electrodes (Table S2). In addition to the excellent electrical conductivity, the ultrathin thickness of the Ti_3C_2 nanosheets could provide a high specific surface area for enzyme immobilization. As the enzyme molecules were immobilized on the nanosheet surface, the active sites of the immobilized enzyme were highly accessible from exterior environments, thereby improving the sensitivity of the biosensor. Stability of the biosensors was investigated through scanning the Ti_3C_2-PLL-GOx/GCE electrode for 100 times under cyclic voltammetry. It was found that the current was maintained at more than 85% of the initial current (Figure S6), indicating good stability of the developed glucose biosensor.

Conclusions

In summary, we have developed a hybrid Ti_3C_2-PLL-GOx nanoreactor that could catalyze the cascade reactions of glucose oxidation and the intermediate H_2O_2 decomposition. The PLL modification provide the Ti_3C_2 MXene nanosheets with highly compatible surface for GOx adsorbing (high as 50 wt.%.) and cross-linking. High-performance electrode for glucose electrochemical sensing is obtained through

Journal Pre-proofs

applying the Ti_3C_2-PLL-GOx nanosheets on GCE with a detection limit of 2.6 μM. The calculated detection sensitivity (38.18 μA mM^{-1} cm^{-2}) is much higher than the previously reported GOx/Au/MXene/Nafion/GCE electrode (4.2 μA mM^{-1} cm^{-2}).[65] This work not only enriches the technology of GOx immobilization, but also provides a general yet efficient strategy for the preparation and stabilization of various enzyme-loaded MXenes with high enzyme content and homogeneous enzyme distribution, leading to possible applications in electrochemical devices, biosensing, and biofuel cells.

Conflicts of interest

The authors declare no competing financial interest.

Acknowledgements

This work was financially supported by the National Key R&D Program of China (2018YFC1602301, 2018YFA0209402), and the National Natural Science Foundation of China (21373059).

References

[1] J. S. Y. Chia, M. T. T. Tan, P. S. Khiew, J. K. Chin, C. W. Siong, A bio-electrochemical sensing platform for glucose based on irreversible, non-covalent pi–pi functionalization of graphene produced via a novel, green synthesis method, Sens. Actuators, B 210 (2015) 558-565.

Journal Pre-proofs

[2] M. Del Barrio, R. Cases, V. Cebolla, T. Hirsch, S. de Marcos, S. Wilhelm, J. Galban, A reagentless enzymatic fluorescent biosensor for glucose based on upconverting glasses, as excitation source, and chemically modified glucose oxidase, Talanta 160 (2016) 586-591.

[3] M. Baghayeri, H. Veisi, M. Ghanei-Motlagh, Amperometric glucose biosensor based on immobilization of glucose oxidase on a magnetic glassy carbon electrode modified with a novel magnetic nanocomposite, Sens. Actuators, B 249 (2017) 321-330.

[4] J. Yoon, S. N. Lee, M. K. Shin, H. W. Kim, H. K. Choi, T. Lee, J. W. Choi, Flexible electrochemical glucose biosensor based on GOx/gold/MoS_2/gold nanofilm on the polymer electrode, Biosens. Bioelectron. 140 (2019) 111343.

[5] T. Liang, L. Zou, X. Guo, X. Ma, C. Zhang, Z. Zou, Y. Zhang, F. Hu, Z. Lu, K. Tang, C. Li, Rising mesopores to realize direct electrochemistry of glucose oxidase toward highly sensitive detection of glucose, Adv. Funct. Mater. 29 (2019) 1903026.

[6] C. Fu, D. Yi, C. Deng, X. Wang, W. Zhang, Y. Tang, F. Caruso, Y. Wang, A partially graphitic mesoporous carbon membrane with three dimensionally networked nanotunnels for ultrasensitive electrochemical detection, Chem. Mater. 29 (2017) 5286-5293.

[7] Y. Lin, M. Bariya, H. Y. Y. Nyein, L. Kivimaki, S. Uusitalo, E. Jonsson, W. Ji, Z. Yuan, T. Happonen, C. Liedert, J. Hiltunen, Z. Fan, A. Javey, Porous enzymatic membrane for nanotextured glucose sweat sensors with high stability toward reliable

noninvasive health monitoring, Adv. Funct. Mater. 29 (2019) 1902521.

[8] B. K. Shrestha, R. Ahmad, H. M. Mousa, I. G. Kim, J. I. Kim, M. P. Neupane, C. H. Park, C. S. Kim, High-performance glucose biosensor based on chitosan-glucose oxidase immobilized polypyrrole/Nafion/functionalized multi-walled carbon nanotubes bio-nanohybrid film, J. Colloid Interface Sci. 482 (2016) 39-47.

[9] A. Soni, S. K. Jha, A paper strip based non-invasive glucose biosensor for salivary analysis, Biosens. Bioelectron. 67 (2015) 763-768.

[10] Y. Zhang, J. Wang, J. Yu, D. Wen, A. R. Kahkoska, Y. Lu, X. Zhang, J. B. Buse, Z. Gu, Bioresponsive microneedles with a sheath structure for H_2O_2 and pH cascade-triggered insulin delivery, Small 14 (2018) 1704181.

[11] X. Liu, Y. Liu, J. Wang, T. Wei, Z. Dai, Mild hyperthermia-enhanced enzyme-mediated tumor cell chemodynamic therapy, ACS Appl. Mater. Interfaces 11 (2019) 23065-23071.

[12] W. Pan, B. Cui, P. Gao, Y. Ge, N. Li, B. Tang, A cancer cell membrane-camouflaged nanoreactor for enhanced radiotherapy against cancer metastasis, Chem. Commun. 56 (2020) 547-550.

[13] S. M. Jo, F. R. Wurm, K. Landfester, Oncolytic nanoreactors producing hydrogen peroxide for oxidative cancer therapy, Nano Lett. 20 (2020) 526-533.

[14] C. Abreu, Y. Nedellec, O. Ondel, F. Buret, S. Cosnier, A. Le Goff, M. Holzinger, Glucose oxidase bioanodes for glucose conversion and H_2O_2 production for horseradish peroxidase biocathodes in a flow through glucose biofuel cell design, J. Power Sources

392 (2018) 176-180.

[15] B. Mecheri, D. De Porcellinis, P. T. Campana, A. Rainer, M. Trombetta, A. Marletta, O. N. Oliveira, Jr., S. Licoccia, Tuning structural changes in glucose oxidase for enzyme fuel cell applications, ACS Appl. Mater. Interfaces 7 (2015) 28311-28318.

[16] Z. Gu, A. A. Aimetti, Q. Wang, T. T. Dang, Y. Zhang, O. Veiseh, H. Cheng, R. S. Langer, D. G. Anderson, Injectable nano-network for glucose-mediated insulin delivery, ACS Nano 7 (2013) 4194-4201.

[17] M. Christwardana, Y. Chung, Y. Kwon, Co-immobilization of glucose oxidase and catalase for enhancing the performance of a membraneless glucose biofuel cell operated under physiological conditions, Nanoscale 9 (2017) 1993-2002.

[18] L. Xin, C. Zhou, Z. Yang, D. Liu, Regulation of an enzyme cascade reaction by a DNA machine, Small 9 (2013) 3088-3091.

[19] M. Wang, D. M. Wang, Q. Chen, C. X. Li, Z. Q. Li, J. Lin, Recent advances in glucose-oxidase-based nanocomposites for tumor therapy, Small 15 (2019) 1903895.

[20] M. Naguib, V. N. Mochalin, M. W. Barsoum, Y. Gogotsi, 25th anniversary article: MXenes: a new family of two-dimensional materials, Adv. Mater. 26 (2014) 992-1005.

[21] A. Lipatov, H. Lu, M. Alhabeb, B. Anasori, A. Gruverman, Y. Gogotsi, A. Sinitskii, Elastic properties of 2D $Ti_3C_2T_x$ MXene monolayers and bilayers, Sci. Adv. 4 (2018) eaat0491.

[22] M. Hu, Z. Li, H. Zhang, T. Hu, C. Zhang, Z. Wu, X. Wang, Self-assembled $Ti_3C_2T_x$ MXene film with high gravimetric capacitance, Chem. Commun. 51 (2015) 13531-

13533.

[23] D. Xiong, X. Li, Z. Bai, S. Lu, Recent advances in layered $Ti_3C_2T_x$ MXene for electrochemical energy storage, Small 14 (2018) 1703419.

[24] L. Lorencova, T. Bertok, E. Dosekova, A. Holazova, D. Paprckova, A. Vikartovska, V. Sasinkova, J. Filip, P. Kasak, M. Jerigova, D. Velic, K. A. Mahmoud, J. Tkac, Electrochemical performance of $Ti_3C_2T_x$ MXene in aqueous media: towards ultrasensitive H_2O_2 sensing, Electrochim. Acta 235 (2017) 471-479.

[25] J. Li, Q. Zhang, Y. Zou, Y. Cao, W. Cui, F. Dong, Y. Zhou, Ti_3C_2 MXene modified g-C_3N_4 with enhanced visible-light photocatalytic performance for NO purification, J. Colloid Interface Sci. 575 (2020) 443-451.

[26] Q. Tang, Z. Sun, S. Deng, H. Wang, Z. Wu, Decorating g-C_3N_4 with alkalinized Ti_3C_2 MXene for promoted photocatalytic CO_2 reduction performance, J. Colloid Interface Sci. 564 (2020) 406-417.

[27] Z. Wang, J. Bai, H. Xu, G. Chen, S. Kang, X. Li, Synthesis of three-dimensional Sn@Ti_3C_2 by layer-by-layer self-assembly for high-performance lithium-ion storage, J. Colloid Interface Sci. 577 (2020) 329-336.

[28] M. Soleymaniha, M. A. Shahbazi, A. R. Rafieerad, A. Maleki, A. Amiri, Promoting role of mxene nanosheets in biomedical sciences: therapeutic and biosensing innovations, Adv. Healthcare Mater. 8 (2019) 1801137.

[29] F. Shahzad, M. Alhabeb, C. B. Hatter, B. Anasori, S. Man Hong, C. M. Koo, Y. Gogotsi, Electromagnetic interference shielding with 2D transition metal carbides

(MXenes), Science 353 (2016) 1137-1140.

[30] Y. Cai, J. Shen, G. Ge, Y. Zhang, W. Jin, W. Huang, J. Shao, J. Yang, X. Dong, Stretchable $Ti_3C_2T_x$ MXene/carbon nanotube composite based strain sensor with ultrahigh sensitivity and tunable sensing range, ACS Nano 12 (2018) 56-62.

[31] H. Liu, C. Duan, C. Yang, W. Shen, F. Wang, Z. Zhu, A novel nitrite biosensor based on the direct electrochemistry of hemoglobin immobilized on MXene-Ti_3C_2, Sens. Actuators, B 218 (2015) 60-66.

[32] A. Shahzad, K. Rasool, W. Miran, M. Nawaz, J. Jang, K. A. Mahmoud, D. S. Lee, Two-dimensional $Ti_3C_2T_X$ MXene nanosheets for efficient copper removal from water, ACS Sustainable Chem. Eng. 5 (2017) 11481-11488.

[33] M. Naguib, M. Kurtoglu, V. Presser, J. Lu, J. Niu, M. Heon, L. Hultman, Y. Gogotsi, M. W. Barsoum, Two-dimensional nanocrystals produced by exfoliation of Ti_3AlC_2, Adv. Mater. 23 (2011) 4248-4253.

[34] P. Srivastava, A. Mishra, H. Mizuseki, K. R. Lee, A. K. Singh, Mechanistic insight into the chemical exfoliation and functionalization of Ti_3C_2 MXene, ACS Appl. Mater. Interfaces 8 (2016) 24256-24264.

[35] K. Montazeri, M. Currie, L. Verger, P. Dianat, M. W. Barsoum, B. Nabet, Beyond gold: spin-coated Ti_3C_2-based MXene photodetectors, Adv. Mater. 31 (2019) 1903271.

[36] L. Lorencova, T. Bertok, J. Filip, M. Jerigova, D. Velic, P. Kasak, K. A. Mahmoud, J. Tkac, Highly stable $Ti_3C_2T_x$ (MXene)/Pt nanoparticles-modified glassy carbon electrode for H_2O_2 and small molecules sensing applications, Sens. Actuators, B 263

(2018) 360-368.

[37] F. Wang, C. Yang, M. Duan, Y. Tang, J. Zhu, TiO_2 nanoparticle modified organ-like Ti_3C_2 MXene nanocomposite encapsulating hemoglobin for a mediator-free biosensor with excellent performances, Biosens. Bioelectron. 74 (2015) 1022-1028.

[38] Y. Liu, A. P. F. Turner, M. J. Zhao, W. C. Mak, Processable enzyme-hybrid conductive polymer composites for electrochemical biosensing, Biosens. Bioelectron. 100 (2018) 374-381.

[39] H. Lin, Y. Wang, S. Gao, Y. Chen, J. Shi, Theranostic 2D tantalum carbide (MXene), Adv. Mater. 30 (2018) 1703284.

[40] M. Ghidiu, M. R. Lukatskaya, M. Q. Zhao, Y. Gogotsi, M. W. Barsoum, Conductive two-dimensional titanium carbide 'clay' with high volumetric capacitance, Nature 516 (2014) 78-81.

[41] J. Sun, J. Ge, W. Liu, M. Lan, H. Zhang, P. Wang, Y. Wang, Z. Niu, Multi-enzyme co-embedded organic-inorganic hybrid nanoflowers: synthesis and application as a colorimetric sensor, Nanoscale 6 (2014) 255-262.

[42] Z. H. Chen, C. Q. Chen, H. W. Huang, F. Luo, L. H. Guo, L. Zhang, Z. Y. Lin, G. N. Chen, Target-induced horseradish peroxidase deactivation for multicolor colorimetric assay of hydrogen sulfide in rat brain microdialysis, Anal. Chem. 90 (2018) 6222-6228.

[43] C. Shan, H. Yang, D. Han, Q. Zhang, A. Ivaska, L. Niu, Water-soluble graphene covalently functionalized by biocompatible poly-L-lysine, Langmuir 25 (2009) 12030-

12033.

[44] M. C. Rodriguez, J. Sandoval, L. Galicia, S. Gutierrez, G. A. Rivas, Highly selective determination of uric acid in the presence of ascorbic acid at glassy carbon electrodes modified with carbon nanotubes dispersed in polylysine, Sens. Actuators, B 134 (2008) 559-565.

[45] C. X. Wang, L. M. Chen, P. J. Wang, M. S. Li, D. F. Liu, A novel ultrasensitive electrochemiluminescence biosensor for glutathione detection based on poly-L-lysine as co-reactant and graphene-based poly(luminol/aniline) as nanoprobes, Biosens. Bioelectron. 133 (2019) 154-159.

[46] X. B. Feng, N. Gan, H. R. Zhang, T. H. Li, Y. T. Cao, F. T. Hu, Q. L. Jiang, Ratiometric biosensor array for multiplexed detection of microRNAs based on electrochemiluminescence coupled with cyclic voltammetry, Biosens. Bioelectron. 75 (2016) 308-314.

[47] O. Mashtalir, M. Naguib, V. N. Mochalin, Y. Dall'Agnese, M. Heon, M. W. Barsoum, Y. Gogotsi, Intercalation and delamination of layered carbides and carbonitrides, Nat. Commun. 4 (2013) 1-7.

[48] W. C. Huang, L. P. Hu, Y. F. Tang, Z. J. Xie, H. Zhang, Recent advances in functional 2D MXene-based nanostructures for next-generation devices, Adv. Funct. Mater. 4 (2020) 2005223.

[49] G. Cai, Z. Yu, P. Tong, D. Tang, Ti_3C_2 MXene quantum dot-encapsulated liposomes for photothermal immunoassays using a portable near-infrared imaging

camera on a smartphone, Nanoscale 11 (2019) 15659-15667.

[50] Z. H. Pan, F. Cao, X. Hu, X. H. Ji, A facile method for synthesizing CuS decorated Ti_3C_2 MXene with enhanced performance for asymmetric supercapacitors, J. Mater. Chem. A 7 (2019) 10815-10815.

[51] S. Shen, T. Ke, K. Rajavel, K. Yang, D. Lin, Dispersibility and photochemical stability of delaminated mxene flakes in water, Small 16 (2020) 2002433.

[52] X. Wang, X. Shen, Y. Gao, Z. Wang, R. Yu, L. Chen, Atomic-scale recognition of surface structure and intercalation mechanism of Ti_3C_2X, J. Am. Chem. Soc. 137 (2015) 2715-2721.

[53] W. Tian, A. VahidMohammadi, Z. Wang, L. Ouyang, M. Beidaghi, M. M. Hamedi, Layer-by-layer self-assembly of pillared two-dimensional multilayers, Nat. Commun. 10 (2019) 2558.

[54] M. Hu, Z. Li, T. Hu, S. Zhu, C. Zhang, X. Wang, High-capacitance mechanism for $Ti_3C_2T_x$ mxene by in situ electrochemical Raman spectroscopy investigation, ACS Nano 10 (2016) 11344-11350.

[55] L. Y. Xiu, Z. Y. Wang, M. Z. Yu, X. H. Wu, J. S. Qiu, Aggregation-resistant 3D MXene-based architecture as efficient bifunctional electrocatalyst for overall water splitting, ACS Nano 12 (2018) 8017-8028.

[56] G. Liu, J. Zou, Q. Tang, X. Yang, Y. Zhang, Q. Zhang, W. Huang, P. Chen, J. Shao, X. Dong, Surface modified Ti_3C_2 MXene nanosheets for tumor targeting photothermal/photodynamic/chemo synergistic therapy, ACS Appl. Mater. Interfaces 9

(2017) 40077-40086.

[57] Y. Wang, L. Yu, Z. Zhu, J. Zhang, J. Zhu, C. Fan, Improved enzyme immobilization for enhanced bioelectrocatalytic activity of glucose sensor, Sens. Actuators, B 136 (2009) 332-337.

[58] Y. Wang, F. Caruso, Mesoporous silica spheres as supports for enzyme immobilization and encapsulation, Chem. Mater. 17 (2005) 953-961.

[59] Y. Wang, F. Caruso, Nanoporous protein particles through templating mesoporous silica spheres, Adv. Mater. 18 (2006) 795-800.

[60] Q. Wang, X. Zhang, L. Huang, Z. Zhang, S. Dong, GOx@ZIF-8(NiPd) nanoflower: an artificial enzyme system for tandem catalysis, Angew. Chem., Int. Ed. Engl. 56 (2017) 16082-16085.

[61] P. Bollella, F. Mazzei, G. Favero, G. Fusco, R. Ludwig, L. Gorton, R. Antiochia, Improved DET communication between cellobiose dehydrogenase and a gold electrode modified with a rigid self-assembled monolayer and green metal nanoparticles: The role of an ordered nanostructuration, Biosens. Bioelectron. 88 (2017) 196-203.

[62] X. Lu, H. Zhang, Y. Ni, Q. Zhang, J. Chen, Porous nanosheet-based ZnO microspheres for the construction of direct electrochemical biosensors, Biosens. Bioelectron. 24 (2008) 93-98.

[63] J. Qiu, H. Peng, R. Liang, X. Xia, Facile preparation of magnetic core-shell Fe_3O_4@Au nanoparticle/myoglobin biofilm for direct electrochemistry, Biosens. Bioelectron. 25 (2010) 1447-1453.

[64] J. Liu, X. Jiang, R. Zhang, Y. Zhang, L. Wu, W. Lu, J. Li, Y. Li, H. Zhang, MXene-enabled electrochemical microfluidic biosensor: applications toward multicomponent continuous monitoring in whole blood, Adv. Funct. Mater. 29 (2019) 1807326.

[65] R. B. Rakhi, P. Nayak, C. Xia, H. N. Alshareef, Novel amperometric glucose biosensor based on MXene nanocomposite, Sci. Rep. 6 (2016) 1-10.

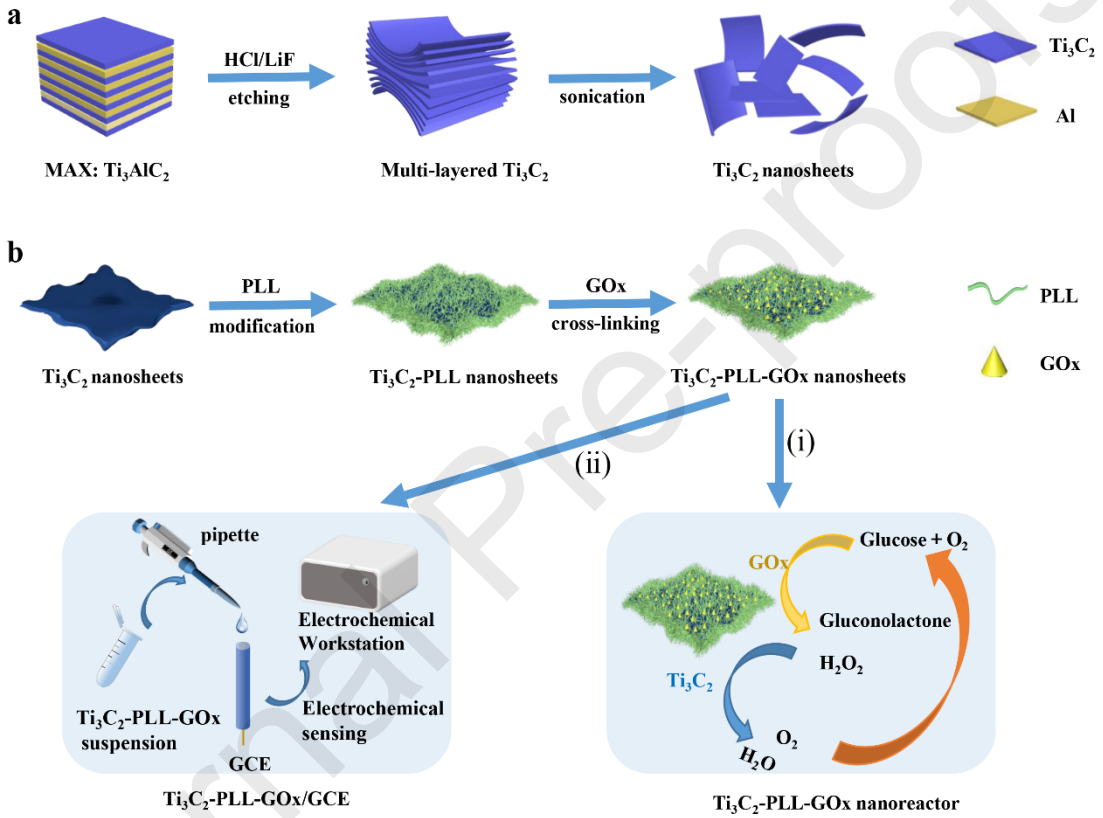

Scheme 1. Schematic illustration of the formation of Ti_3C_2-PLL-GOx nanoreactor. (a) The Ti_3C_2 MXene nanosheets were obtained after etching of the Al layer from the MAX phase Ti_3AlC_2. (b) PLL and GOx were sequentially assembled on the Ti_3C_2 nanosheets and the obtained Ti_3C_2-PLL-GOx was applied for cascade glucose oxidation (i) and electrochemical glucose sensing (ii).

Journal Pre-proofs

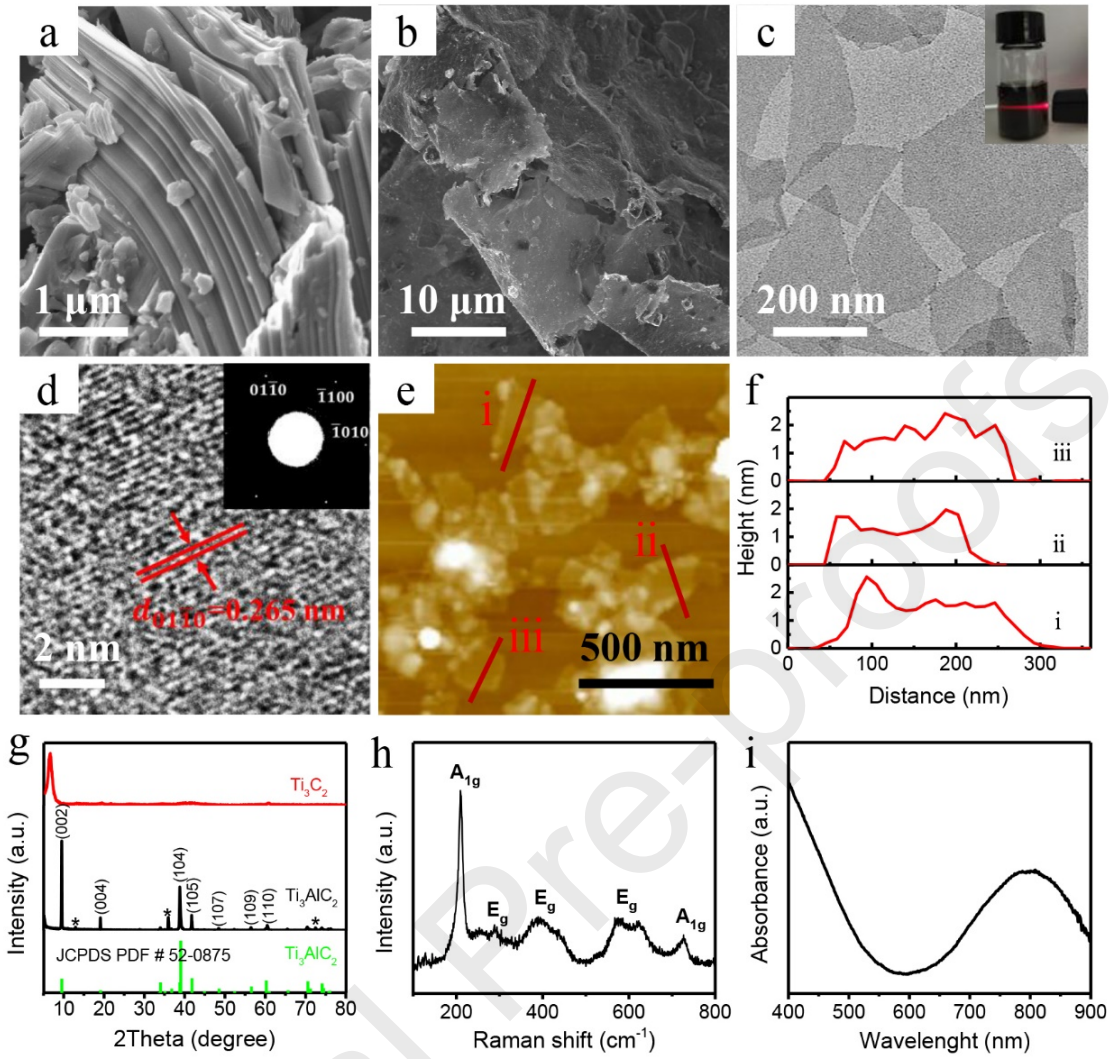

Figure 1. SEM images of the (a) MAX phase Ti_3AlC_2 and (b) multilayered Ti_3C_2 flakes. (c) TEM image of the ultra-thin Ti_3C_2 nanosheets. The inserted digital photograph shows the Tyndall effect with a red laser beam pointed at the Ti_3C_2 suspension. (d) HRTEM image of Ti_3C_2 nanosheets. The insert is SAED image of the Ti_3C_2 nanosheets. (e) AFM image and the (f) thickness and width profiles of Ti_3C_2 nanosheets marked in the AFM image. (g) XRD patterns of Ti_3AlC_2 and Ti_3C_2 nanosheets. (h) Raman spectrum of the Ti_3C_2 nanosheets. (i) UV-vis spectrum of the Ti_3C_2 MXene suspension in water.

Journal Pre-proofs

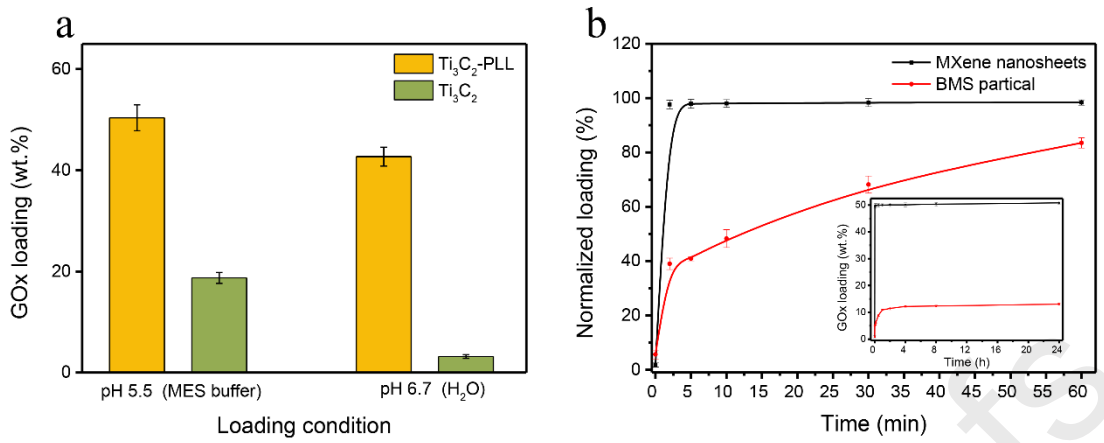

Figure 2. (a) Influence of solution pH on GOx loading on the Ti_3C_2-PLL nanosheets and Ti_3C_2 nanosheets, respectively. (b) Comparison of GOx loading capacity on the 2D Ti_3C_2 nanosheets and 3D porous BMS particles (insert is the GOx adsorption isotherms on the substrates). Each experiment was conducted in triplicate and error bars showed the expected standard deviation at each point.

Journal Pre-proofs

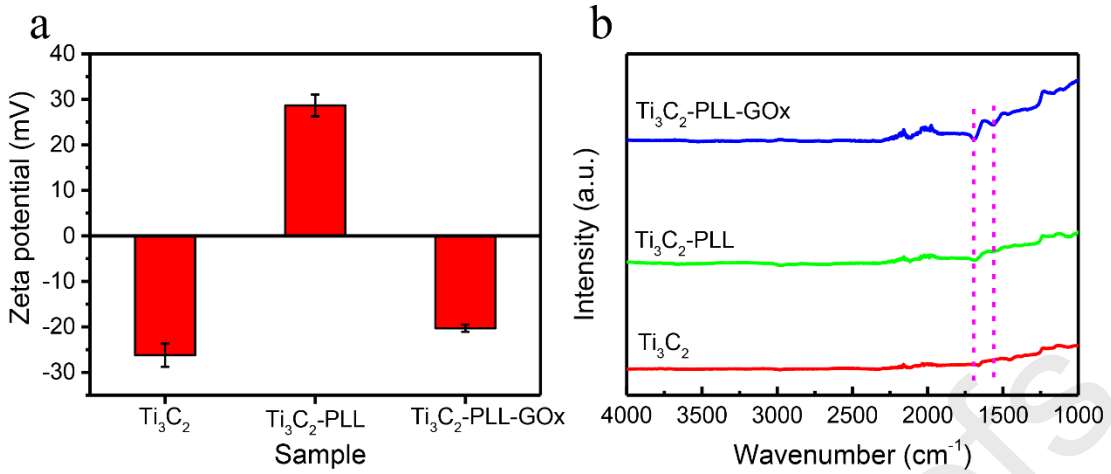

Figure 3. (a) Zeta potential and (b) FTIR spectra of the Ti_3C_2, Ti_3C_2-PLL and Ti_3C_2-PLL-GOx nanosheets.

Journal Pre-proofs

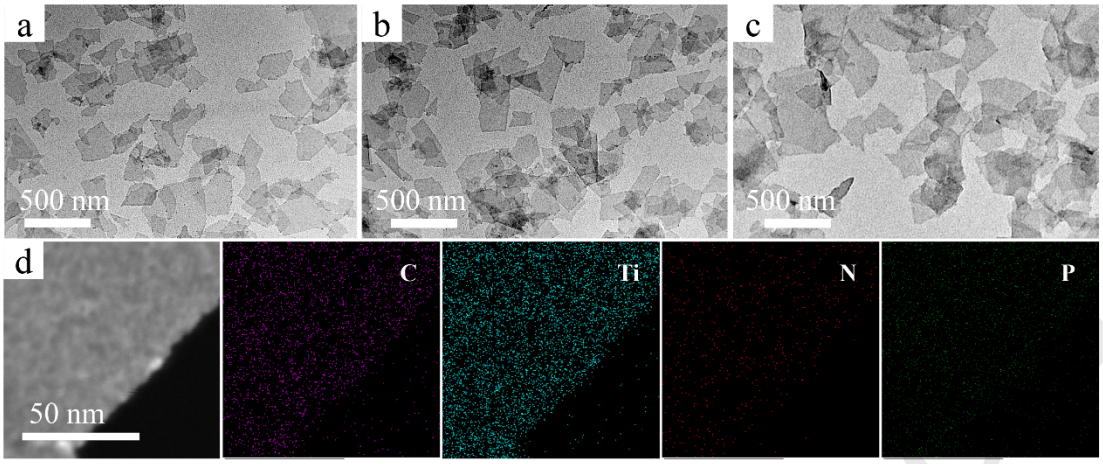

Figure 4. TEM images of (a) Ti_3C_2, (b) Ti_3C_2-PLL, and (c) Ti_3C_2-PLL-GOx nanosheets.

(d) Elemental mapping profiles of the Ti_3C_2-PLL-GOx nanosheets.

Journal Pre-proofs

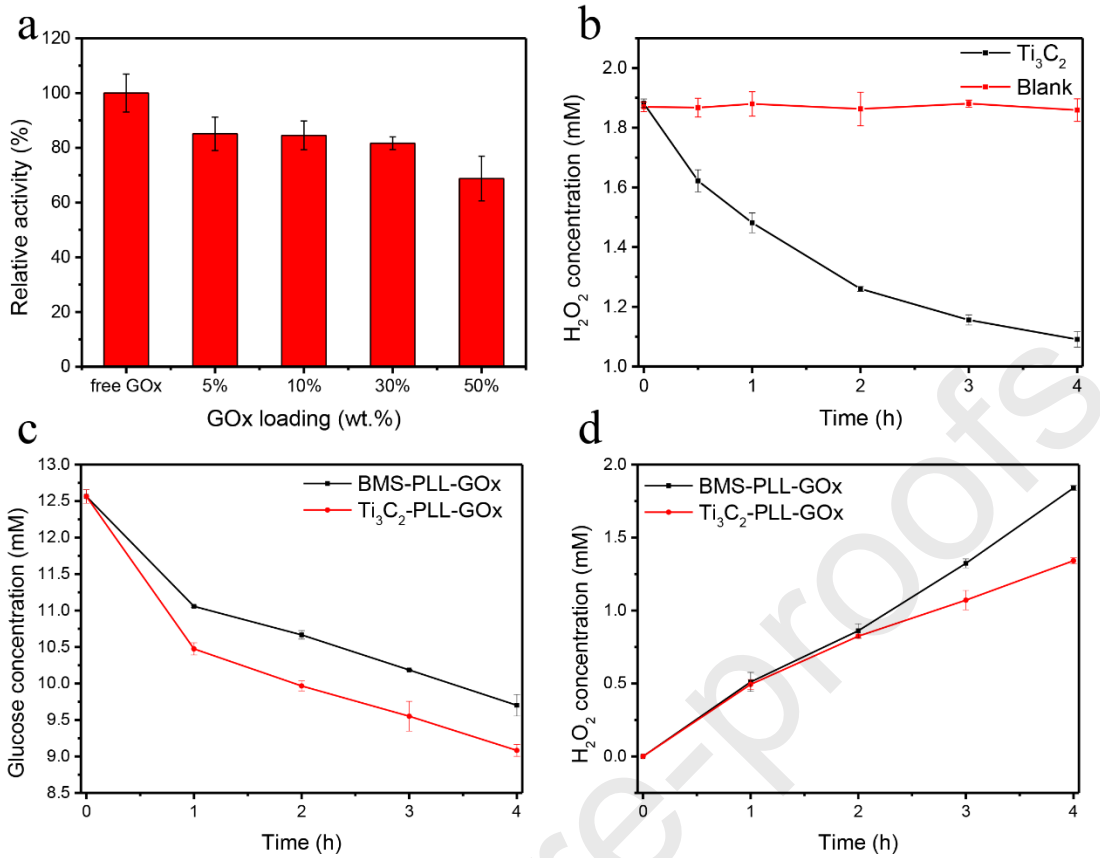

Figure 5. (a) Relative activity of free GOx and Ti_3C_2-PLL-GOx with different GOx loading (5, 10, 30, and 50 wt.%). (b) Decomposition profile of H_2O_2 under the catalyst of Ti_3C_2 nanosheets. (c) Decomposition profiles of glucose under the catalyst of Ti_3C_2-PLL-GOx and BMS-PLL-GOx. (d) H_2O_2 concentrations detected in course of the glucose decomposition reactions plotted in (c). Each experiment was conducted in triplicate and error bars showed the expected standard deviation at each point.

Journal Pre-proofs

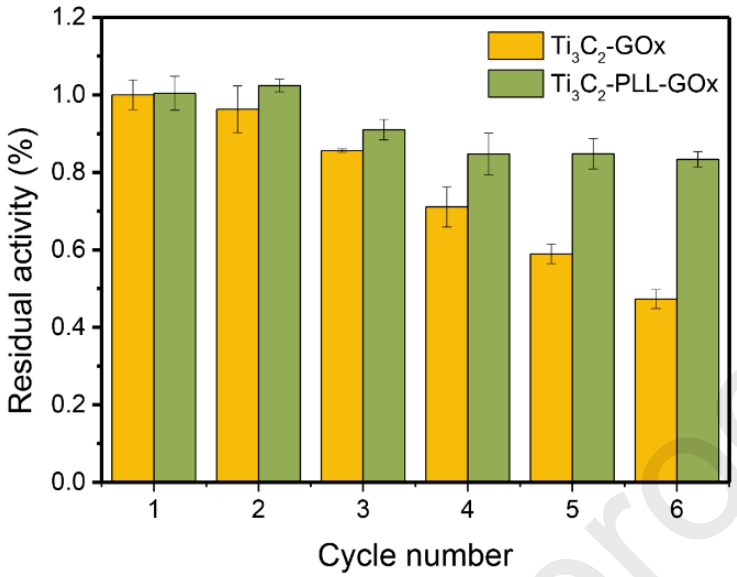

Figure 6. Relative activity of GOx immobilized on Ti_3C_2 and Ti_3C_2-PLL as a function of successive batch reactions. Each experiment was conducted in triplicate and error bars showed the expected standard deviation at each point.

Journal Pre-proofs

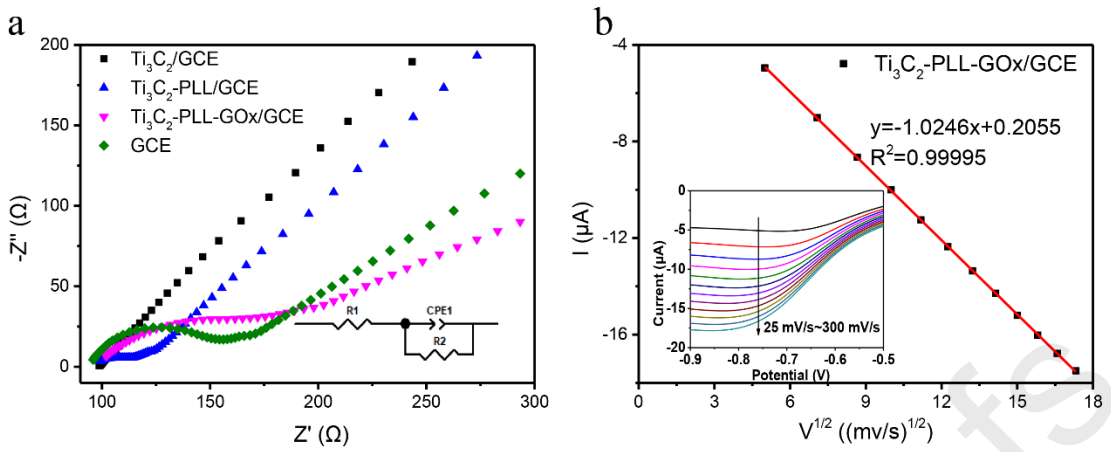

Figure 7. (a) Electrochemical impedance spectroscopy of the GCE, Ti_3C_2/GCE, Ti_3C_2-PLL/GCE, and Ti_3C_2-PLL-GOx/GCE electrodes. The illustration is the corresponding fitted circuit diagram. (b) The linear relationship indicates that the current is proportional to the half power of the scan rate on the Ti_3C_2-PLL-GOx/GCE electrode in the cyclic voltammetry. The insert is the related cyclic voltammogram.

Journal Pre-proofs

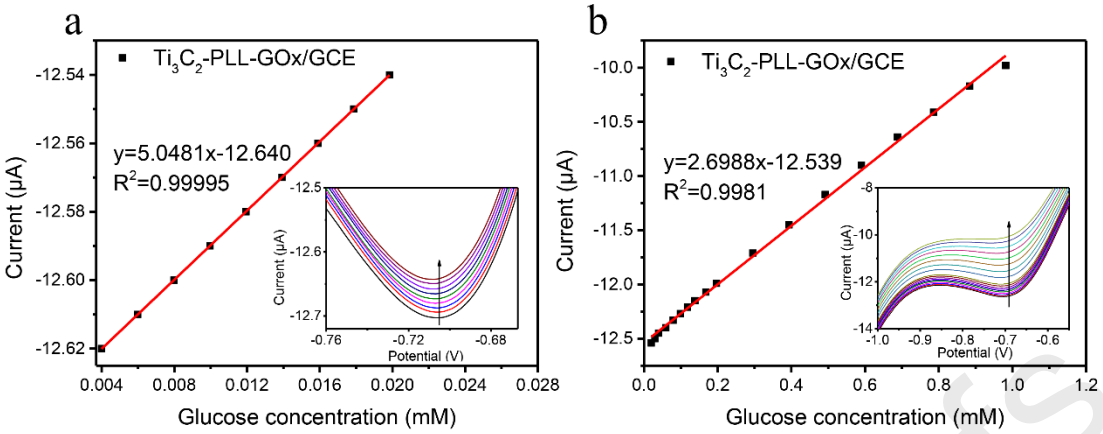

Figure 8. Linear correlation plots between current and glucose concentration obtained from the Ti_3C_2-PLL-GOx/GCE electrodes with glucose concentration in ranges of (a) 4.0-20 μM and (b) 0.02-1.1 mM. The inserts are CV response of glucose at different concentrations.

Journal Pre-proofs

Credit author statement

Minying Wu: Data curation, Writing-Original draft preparation. **Qian Zhang:** Methodology, Investigation. **Yuanyuan Fang:** Methodology, Investigation. **Chao Deng:** Project administration, Writing - Review & Editing. **Fangzhou Zhou**: Visualization, Investigation. **Yi Zhang:** Methodology, Writing- Reviewing and Editing. **Xingdong Wang**: Writing- Reviewing and Editing. **Yi Tang:** Funding acquisition, Supervision. **Yajun Wang:** Funding acquisition, Methodology, Writing-Reviewing and Editing.

Journal Pre-proofs

Declaration of interests

☒ The authors declare that they have no known competing financial interests or personal relationships that could have appeared to influence the work reported in this paper.

☐The authors declare the following financial interests/personal relationships which may be considered as potential competing interests:

Journal Pre-proofs

Graphical Abstract

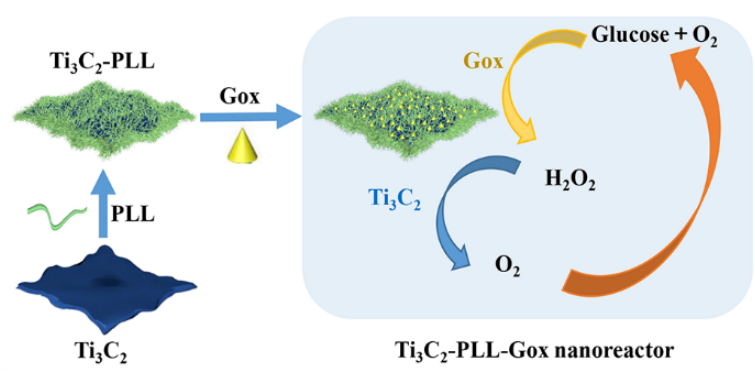

Journal Pre-proofs

Highlights

1. Two-dimensional nanoreactors with cascade catalytic properties in glucose decomposition are prepared via immobilizing glucose oxidase (GOx) on Ti_3C_2 MXene nanosheets.
2. The poly-L-lysine (PLL) modification provides the Ti_3C_2 nanosheets with a highly compactible surface for GOx immobilization with an enzyme loading high as 50 wt.%.
3. Superior enzymatic activity and stability are obtained in the GOx-conjugated Ti_3C_2-PLL nanosheets.
4. The hybrid Ti_3C_2-PLL-GOx nanosheets are applied to construct a high-performance glucose sensor with a detection limit of 2.6 μM.

Journal Pre-proofs